ISSN 0031-918X, Physics of Metals and Metallography, 2021, Vol. 122, No. 13, pp. 1272–1278. © Pleiades Publishing, Ltd., 2021.
ISSN 0031-918X, Physics of Metals and Metallography, 2021. © Pleiades Publishing, Ltd., 2021.

ELECTRICAL AND MAGNETIC PROPERTIES

The Preservation of the Half-Metallicity during the Substitution of Manganese in $Ba_{1-x}Mn_xO$ Alloy

R. Chaala[a], D. Bensaid[b, c, *], B. Doumi[d], S. Hebri[c], N. Bouzouira[b], and Y. Azzaz[a, b]

[a] *Physics Department, University of Sidi-Bel-Abbes, Sidi-Bel-Abbes, 22000 Algeria*

[b] *Laboratory Physico-Chemistry of Advanced Materials, University of Djillali Liabes, Sidi-Bel-Abbes, 22000 Algeria*

[c] *Institute of Sciences, University Belhadj Bouchaib, Ain-Temouchent, 46000 Algeria*

[d] *Faculty of Sciences, Department of Physics, Dr. Tahar Moulay University of Saïda, Saïda, 20000 Algeria*

**e-mail: djillali.bensaid@cuniv-aintemouchent.dz*

Received March 28, 2020; revised July 20, 2020; accepted August 4, 2020

Abstract—The object of this study is to investigate the half-metallicity, electronic structures and magnetic in the $Ba_{1-x}Mn_xO$ compounds under the effect of substitution of Mn impurity at the different composition $x =$ 0.25, 0.5, and 0.75 by the use of density functional theory (DFT) based first principle calculations. The half-metallic ferromagnetism is explained by analyzing the density of states. The ferromagnetic states configuration is originated from the 3*d*-eg (Mn) partially filled states associated with *p*–*d* exchange mechanism. For the three concentrations, the total magnetic moment is integral member, which is mainly contributed by the magnetic moment Mn atom. We have found that $Ba_{0.75}Mn_{0.25}O$, $Ba_{0.5}Mn_{0.5}O$ and $Ba_{0.25}Mn_{0.75}O$ compounds have direct half-metallic ferromagnetic gaps of 0.834, 0.58 and 0.368 eV, respectively, which decrease with increasing Mn concentration. Therefore, the $Ba_{1-x}Mn_xO$ materials seem to be potential candidates for possible applications of semiconductor spintronics.

Keywords: FP-LAPW method, Mn doped BaO, ferromagnetism, electronic structures, spintronics applications

DOI: 10.1134/S0031918X20140057

INTRODUCTION

The spintronics technology is a modern field of electronics, which has various advantages over conventional electronics. The spintronics use the spin of electron in addition to it charge in electronic devices because low energy is required to manipulate the spin orientation.

Spintronics has many potential beneficial applications for spintronics-based transistors, for example the ability to integrate data process and storage at the same time and controlling of spin currents with an external magnetic field. Among the spintronics applications, the ferromagnetic electrodes that serve as reservoirs of spin-polarized electrons from which nonequilibrium spin population is injected in a typically nonmagnetic or insulating material. These polarized spins are then transferred within times typically shorter than their characteristic spin relaxation time through aforementioned nonmagnetic or insulating material and finally detected at another ferromagnetic or superconducting electrode [1], that is the concept of spin-field effect transistor (spin-FET) has been proposed by Datta and Das the "Datta-Das" spin modulator [2].

In ferromagnetic semiconductors doped with small fraction of the magnetic impurities such as ions of manganese (Mn), each magnetic ion is substituted on a cationic site and induces a local magnetic moment, as well as an extra hole due to the mismatch of the electronic structure of the two ions. These holes are weakly correlated to the acceptor ions and circulate throughout the system. They interact with the magnetic ions, *d* orbitals via the *p*–*d* hybridization. Among the recent work which treats the effect of defects resulting from the substitution of transition metals in a semiconductor, we can cite the study of Ivády et al., [3], which analyzes the correction of the hybrid function HSE06 on the possibility of locating defect states.

In literature, several ferromagnetic semiconductors such as EuS, EuO, $CdCr_2S_4$ and $CdCr_2Se_4$ [4], $Ga_{1-x}Mn_xN$ [5–7], $Ba_{1-x}Cr_xO$ [8] and $Ba_{1-x}Cr_xSe$ [9] have been studied in order to characterize their electronic and magnetic properties. Besides, some first-principle calculations have been carried out to investigate the phase stability of transition metals implanted in MgO and BaO. Misra et al., [10] found that TM dopants in the BaO are localized on interstitial sites instead of cation sites for a diluted doping limit.

According to Strewlow and Cook [11], the experimental value of the energy gap for BaO is equal to

4.8 eV, whereas, the theoretical values previously found are 2.08 [12], 2 [13], and 1.75 eV [14]. Several experimental and theoretical studies have studied the behavior of the electronic structure of manganese oxide MnO. Kuneš et al., [15] use the LDA + DMFT approach to describe the Mott transition in MnO, which is considered as the example of the canonical Mott insulators and it has the partially filled 3*d* states leading to a spherical magnetic moment. The electronic structure of MnO shifts from metal to an insulator with a change of structural phase under the effect of pressure due to the very sensitive 3*d* bandwidth [15]. According to the study of Pask et al., [16], the MnO is an insulator with an antiferromagnetic order AFII.

Solovyev [17] found that the electronic structure of the narrow band MnO is in good agreement with the photoemission spectra.

The theoretical calculations performed by the Hartree–Fock approximation revealed that the electronic structure of the ground state of MnO has an insulating character with a wide band gap about ~13 eV [18]. On the other hand, the Massidda et al., [19] and Fujimori et al., [20] found that MnO has gap width around ~3.5–4.0 and ~7.5 eV, respectively. This means that most of the theoretical calculations underestimate the experimental energy gap for both BaO and MnO. The high Curie temperature and the growth technology are important features sought in novel diluted magnetic semiconductors (DMS). T. Dietl and al., [21] have used the Zener's model of ferromagnetism to explain Curie temperature (T_C) for various *p*-type zinc-blende magnetic semiconductors, where the magnetism is originated from *sp–d* hybridization.

However, most of the work published on high temperature magnetic order DMS materials has involved *n*-type materials such as Co-doped ZnO or Mn-doped GaN.

Recently, ferromagnetic semiconductors have attracted the intention of the scientific community for new applications of spintronic devices. In this context, we provided a detailed study on a magnetic semiconductor, which has properties suitable for spintronics applications.

The object of this study is to investigate the electronic structures, magnetic properties and half-metallicity in the $Ba_{1-x}Mn_xO$ alloys, using the density functional theory (DFT) [22], where the exchange et correlation potential is treated by the generalized gradient approximation functional of Wu and Cohen [23].

Calculation Details

All calculations were performed using full-potential linearized augmented-plane-wave (FP-LAPW) method [24] as implemented in the WIEN2k package provided by Blaha, Schwartz, and coworkers [25–27]. The Wu and Cohen version of the generalized gradient-approximation (GGA) to the exchange correlation functional of DFT was adopted [23].

Table1. Lattice constants *a*, bulk modulus *B* and its pressure derivative *B'* of $Ba_{1-x}Mn_xO$ ($x = 0.25, 0.5,$ and 0.75)

	a, Å	*B,* GPa	*B'*
$Ba_{0.75}Mn_{0.25}O$	5.3056	87.098	4.35
$Ba_{0.5}Mn_{0.5}O$	5.0811	100.187	4.62
$Ba_{0.25}Mn_{0.75}O$	4.8035	123.33	3.83

The muffin-tin radii were chosen to minimize the interstitial space and ensure that the muffin-tin spheres do not overlap. We have taken the muffin-tin radii (R_{MT}) of 2.59, 2.1, and 2.05 for Ba, O, and Mn atoms, respectively. The $R_{MT} \times K_{max} = 7$ was used for the number of plane waves, and the expansion of the wave functions was set to $l_{max} = 10$ inside of the muffin-tin spheres. The charge density was Fourier expanded up to $G_{max} = 12$ a.u.$^{-1}$, where G_{max} is the largest vector in the Fourier expansion. The $13 \times 13 \times 13$ *k*-points meshes were used for the integration in the sampling Brillouin zone. The energy convergence criterion was set to 10^{-7} Ry.

RESULTS AND DISCUSSIONS

Structural Properties

To characterize the electronic and magnetic properties, we calculate in this section the structural parameters of the $Ba_{1-x}Mn_xO$ alloys at concentrations $x = 0.25$, 0.5 and 0.75, the binary BaO compound has the rock-salt NaCl (B1) structure with space group ($Fm\bar{3}m$) no. 225. We have substituted the Ba_4O_4 supercells of eight atoms by one, two and three Mn atoms at Ba cationic sites to get respectively the concentrations $x = 0.25$, 0.5 and 0.75. We have obtained the $Ba_{0.75}Mn_{0.25}O$ for $x = 0.25$ and $Ba_{0.25}Mn_{0.75}O$ for $x = 0.75$ with cubic structures corresponding to space group of $Pm\bar{3}m$ no. 221, while $Ba_{0.5}Mn_{0.5}O$ supercell for $x = 0.5$ has tetragonal structure with space group of $P4/mmm$ no. 123.

The variations of total energies as a function of equilibrium volumes of $Ba_{1-x}Mn_xO$ compounds are fitted with the empirical Murnaghan's equation of state [28] to determine the structural parameters. The calculated lattice constants (*a*), bulk modules (*B*) and their pressure derivatives (*B'*) of $Ba_{1-x}Mn_xO$ alloys at concentrations $x = 0.25$, 0.5, and 0.75 are summarized in Table 1.

From the Fig. 1, we have depicted that the stiffness increases with decreasing the lattice constant as the

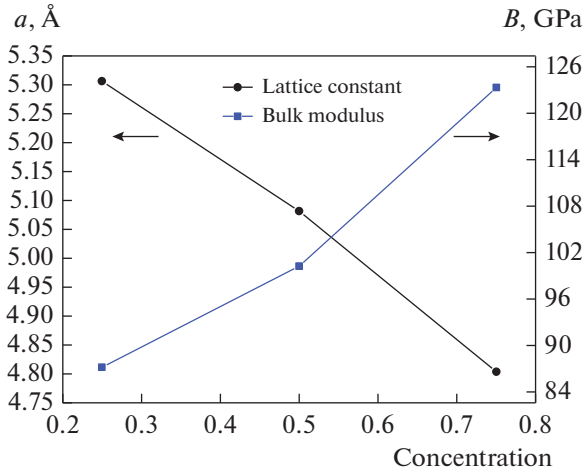

Fig. 1. Variation of lattice constant a (Å) and bulk modulus B (GPa) of $Ba_{1-x}Mn_xO$ as a function of composition x.

concentration of Mn increases. The decrease in the lattice constant is due to the fact that the size of the ionic radius of Mn atom is smaller than that the Ba atom. The same behaviors of lattice constant and bulk modulus were found by Lakhdari et al., [29] for $Ba_{1-x}Cr_xO$ at concentrations $x = 0.25$, 0.5 and 0.75. We have noticed that there are no experimental or theoretical results to compare them with our results.

Electronic Properties

In this section, we have performed the calculations of the electronic structures by the use of computed theoretical values of lattice parameters. The electronic states such as $5p^66s^2$ of Ba, $2s^22p^4$ of O and $4s^23d^5$ of Mn are treated as valence electrons.

To represent the band structure, the energy is calculated as a function of the wave vector by the energy dispersion relation $E(\vec{k})$ in the Brillion zone. Firstly, we have found that our compounds have semiconductor behavior with direct gaps for minority spins because the valence band maxima and the conduction band point minimum occur at the Γ point ($k = 0$), whereas majority spins have a metallic character. From the band structures, it can clearly be seen that the increase in the concentration of the substituted Mn atom has a direct effect on the decrease in the half-metallic ferromagnetic gap of minority spins.

The analysis of electronic structures shows that the rather large shift of the occupied majority d-states for different concentrations is compensated by a shift of the unoccupied minority d-Mn states, which keeps the exchange splitting.

The band structures of $Ba_{1-x}Mn_xO$ at concentrations $x = 0.25$, 0.5 and 0.75 are displayed by Fig. 2.

We can see that the substituting manganese (Mn) impurities in BaO compound have considerable effect

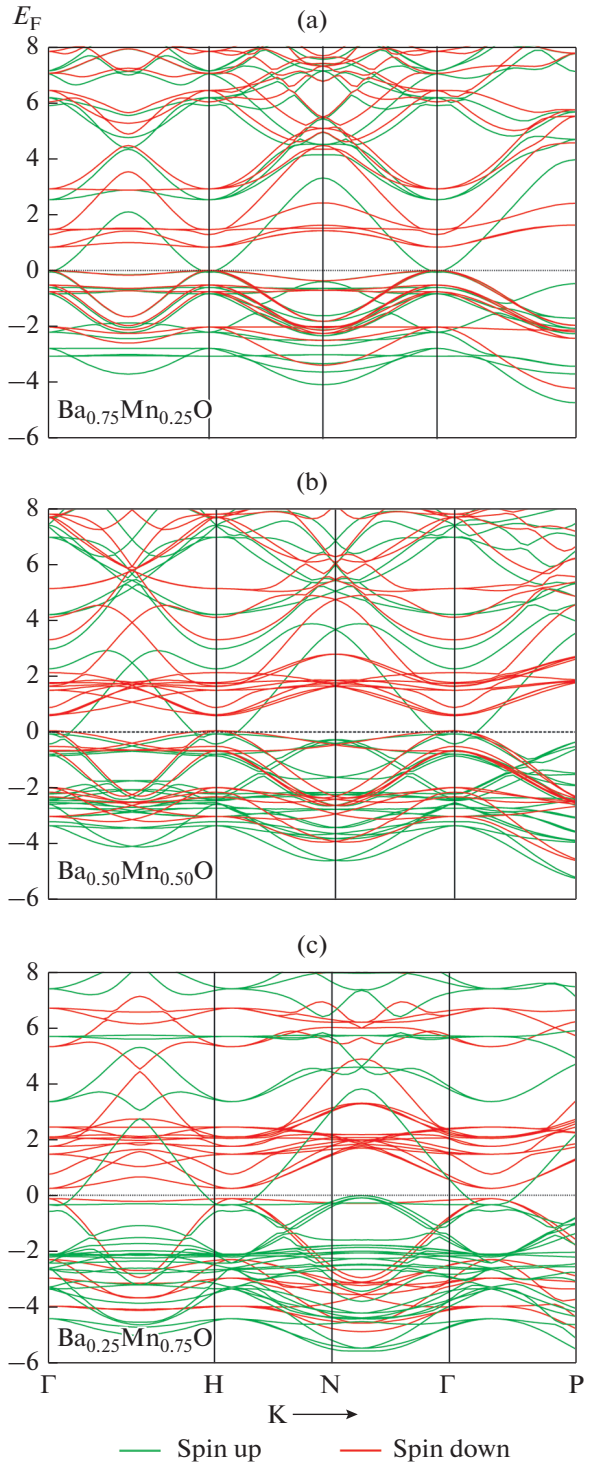

Fig. 2. Band structures of majority spin (red) and minority spin (green) for $Ba_{1-x}Mn_xO$ ($x = 0.25$, 0.5, and 0.75).

on electronic structures. In the case of the minority states, the half metallic gap decreases with increasing Mn concentration. The majority-spin bands are more in number (bands in green colors) than the minority-spin bands (bands in red colors), consequently the

half-metallic ferromagnetic gap (G_{HMF}) and half-metallic gap (G_{HM}) are created in the minority-spin bands (see Fig, 2). The half-metallic gap is an important factor to determine the importance of the DMS [30, 31].

The Density of States

The essential features in spintronic devices are the injection, the transfer and the control of the spin polarized carriers. The half-metallic ferromagnetic materials have an unequal density of states (DOS) of majority-spin and minority-spin states at the Fermi level. In Figs. 3a–3c, we can see that $Ba_{1-x}Mn_xO$ compounds for all concentrations $x = 0.25$, 0.5, and 0.75 have half-metallic ferromagnetic gaps for in minority-spin states. The common point for alloys at different concentrations is that Fermi level is located at the top of the valence band for majority-spin states.

From the DOS of majority-spin states, we can see that the upper part of 3*d*-Mn states centered at −3.05 eV for $Ba_{0.75}Mn_{0.25}O$ are shifted to −2.6 eV for $Ba_{0.5}Mn_{0.5}O$.

After examining the electronic structure in more peculiarity detail, some particular-changes are found. For example, the displacement considerable shift of the occupied majority *d*-states is compensated by a move of the occupied minority *d*-states, and this keeps the exchange splitting rather fixed.

This result is revealed by the splitting of the occupied minority *d*-Mn states (seen at 1.45, 1.77, and 2.05 eV for 0.25, 0.5, and 0.75 Mn composition, respectively) thus, that. The unoccupied *d*-Mn states of the minority spin move toward Fermi level with increasing Mn concentration, and the half-metallic gap is reduced from 0.12 eV for $Ba_{0.75}Mn_{0.25}O$ to 0.044 eV for $Ba_{0.5}Mn_{0.5}O$ to 0.019 eV for $Ba_{0.25}Mn_{0.75}O$. The $Ba_{1-x}Mn_xO$ materials maintain a half-metallic behavior, which make them possible candidates for spintronics applications. our calculations are given in Figs. 3a–3c. Ba-6*s* states are approximately localized in intervals [3, 12] and [−9, −12]. Mn-3*d* states are observed around E_F, we found that the spin polarization at the Fermi level is about 100%. Our findings are encouraging for spintronics applications, due to the robustness of the half-metallicity of our materials.

The disorder improves the resistivity without much reduction in Curie temperature for most types of chemical disorder materials.

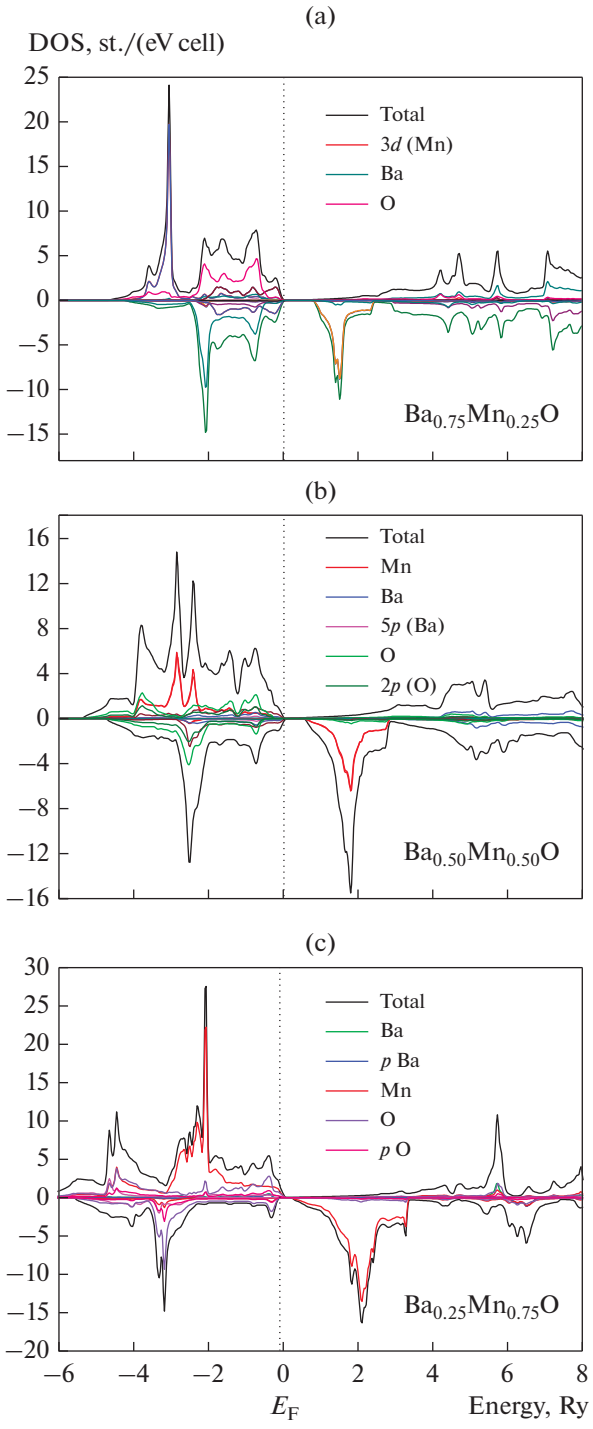

Fig. 3. Total and partial density of states DOS of $Ba_{1-x}Mn_xO$ ($x = 0.25$, 0.5, and 0.75).

Magnetic Properties

We find that the exchange nature in our compound is of the double-exchange type which stabilizes the ferromagnetic state. The exchange splitting has to be larger than the crystal field splitting between t_{2g} and e_g orbitals.

Usually, in the II–VI DMS doped Mn, the intrinsic characteristic is preserved and the exchange coupling of local moments is dominated by the superexchange coupling [32]. Since the magnetic impurity concentration is small in the diluted magnetic semiconductors (DMS), the magnetic interactions in this

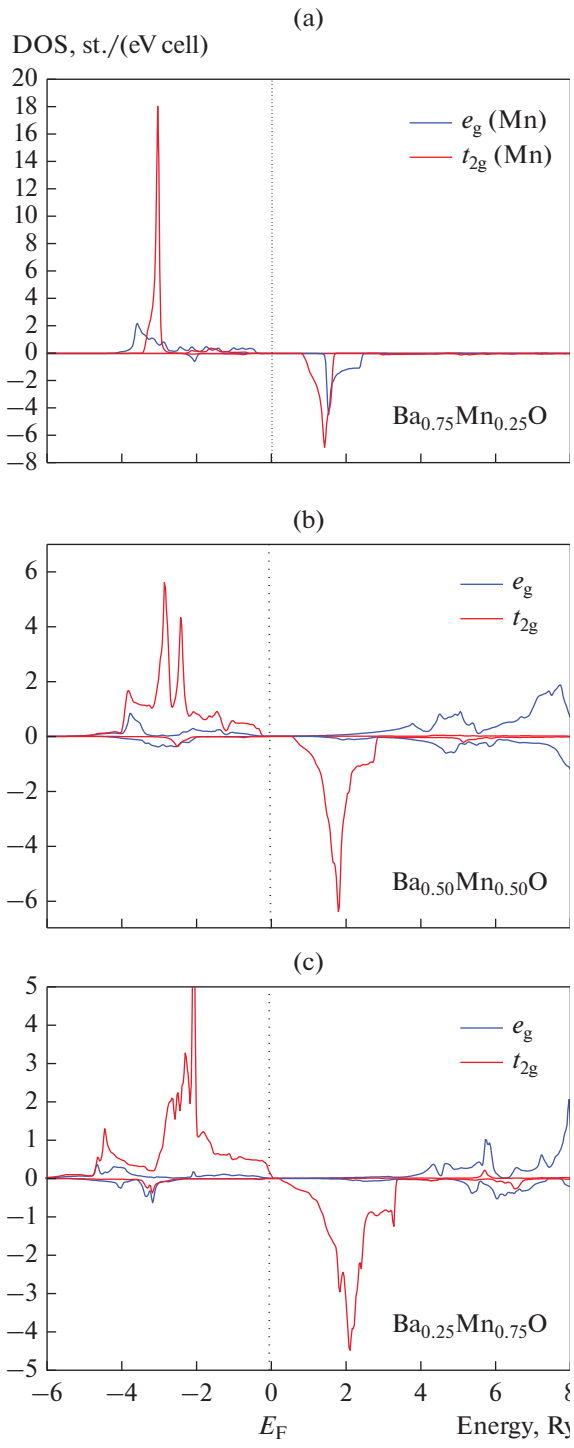

Fig. 4. Density of states of the e_g twofold generate and t_{2g} threefold degenerate DOS for Mn atom of $Ba_{1-x}Mn_xO$ ($x = 0.25$, 0.5, and 0.75).

kind of material are mainly caused by itinerant holes, which align the magnetic moments and create ferromagnetic arrangement. In our compounds, the t_{2g}-d

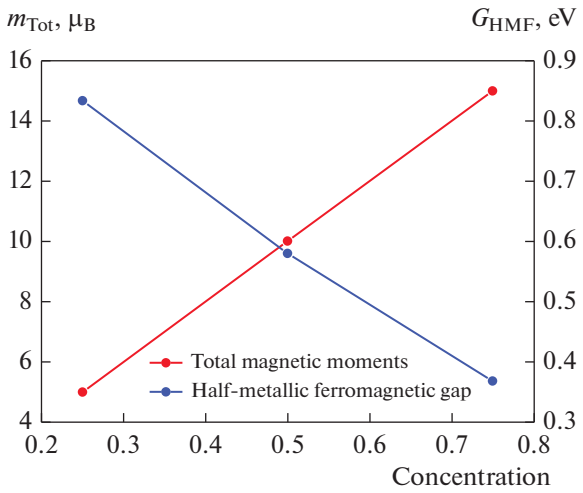

Fig. 5. Variation the half-metallic gap G_{HM} and total magnetic moment of $Ba_{1-x}Mn_xO$ as a function of composition.

(Mn) states occur below the states e_g (Mn) because the atom Mn is situated in the octahedral surroundings.

The 3d-Mn of majority-spin states is located almost below Fermi level (see Figs. 4a–4c), meaning that these states are fully filled. Where the t_{2g} (Mn) majority-spin states are wholly fill with five electrons, yet the e_g (Mn) states are empty (see Figs. 4a–4c). Therefore, the 3d (Mn) states are completely filled by five electrons, which give rise a total magnetic moment of 5 μ_B per Mn atom. The calculated total magnetic moment and the partial magnetic moment of the Ba, O and Mn atoms are summarized in Table 2.

In Table 2, We give the total and partial magnetic moment of the Ba, O, and Mn atoms. From the Table 2, we can draw the following results:

Firstly, it shows that the magnetic moment of the Mn atom is 4.3 μ_B for the three concentrations $x =$ 0.25, 0.5, and 0.75.

Secondly, it is clear that the total magnetic moments are mainly originated from the partial magnetic moments of the Mn atoms, while the contributions of partial magnetic moments of the Ba and O atoms are negligible. We show that the total magnetic moment increases with the increasing Mn concentration by step of 0.01 μ_B for the magnetic moment of Mn (see Fig. 5).

The computed total magnetic moment m_{Tot} and half-metallic ferromagnetic band gap E_g at versus concentration were fitted by the polynomial equation given by the following expressions:

$$\begin{cases} m_{Tot} = -0.058 + 20.264x - 0.24x^2 \\ G_{HMF} = 1.13 - 1.268x + 0.336x^2 \end{cases}$$

Table 2. Calculated total, local magnetic moment, half-metallic ferromagnetic gap G_{HMF} and half-metallic gap G_{HM} of minority-spin bands for $Ba_{1-x}Mn_xO(x = 0.25, 0.5, \text{and } 0.75)$

	$m_{Tot}(\mu_B)$	$m_{Mn}(\mu_B)$	$m_{Ba}(\mu_B)$	$m_O(\mu_B)$	$E_g(G_{HMF})$, eV	G_{hm}, eV
$Ba_{0.75}Mn_{0.25}O$	4.993	4.296	−0.0001	0.0588	0.834	0.019
$Ba_{0.5}Mn_{0.5}O$	10.014	4.306	0.072	0.198	0.580	0.044
$Ba_{0.25}Mn_{0.75}O$	15.005	4.311	0.0048	0.353	0.368	0.12

Exchange Coupling

The DMS material becomes highly disordered due to magnetic impurities that are randomly scattered and that rise the magnetic exchanges interactions. Consequently, As the result, the DMS fall under category of strongly correlated systems where static mean-field approach is too homely to capture the complexity of the material to obtain a magnetic order between the host atoms and the magnetic atom.

It is very useful to treat exchange coupling in DMS by exchange constants, which are important parameters characterizing DMS for spintronic applications.

The *sp*–*d* exchange constant $N_0\alpha$ and $N_0\beta$ are determined from the following mean-field theory expressions [33, 34]:

$$N_0\alpha = \frac{\Delta E_c}{xs} \text{ and } N_0\beta = \frac{\Delta E_v}{xs},$$

where $\Delta E_c = E_c^{\downarrow} - E_c^{\uparrow}$ is the conduction band-edge spin splitting and $\Delta E_v = E_v^{\downarrow} - E_v^{\uparrow}$ is the valence band-edge spin splitting at the Γ symmetry point, x is the concentration of Mn per atom, and s is half magnetization per Mn ion. The results of the exchange constants are displayed by the Table 3. We have noticed that the $N_0\beta$ with the increase of Mn concentration, whereas $N_0\alpha$ decreasing with increasing Mn concentration. The $N_0\alpha$ and $N_0\beta$ parameters are positives for all concentrations. Therefore, the exchange couplings between the 3*d*-Mn and the valence and conduction bands are ferromagnetic. The variation of the exchange constants with the concentration were adjusted by the polynomial equation:

$$\begin{cases} N_0\alpha = 0.362 + 1.264x - 1.872x^2 \\ N_0\beta = -0.039 + 0.602x - 0.424x^2 \end{cases}.$$

the small value of $N_0\alpha$ is due the weak ferromagnetic exchange coupling between the magnetic Mn atoms and the nearest neighbors. This exchange decreases as the concentration of magnetic Mn atoms increases.

Table 3. Calculated conduction and valence band-edge spin splitting ΔE_c and ΔE_v and exchange constants $N_0\alpha$ and $N_0\beta$ for $Ba_{1-x}Mn_xO\,(x = 0.25, 0.5, \text{and } 0.75)$

	$\Delta_x^c(\text{pd})$	$\Delta_x^v(\text{pd})$	$N_0\alpha$	$N_0\beta$
$Ba_{0.75}Mn_{0.25}O$	0.831	0.017	1.561	0.031
$Ba_{0.5}Mn_{0.5}O$	0.604	0.11	0.526	0.102
$Ba_{0.25}Mn_{0.75}O$	0.554	0.195	0.257	0.120

SUMMARY

The results of the our theoretical calculations that we performed using the FP-LAPW method to describe the electronic and magnetic properties of the $Ba_{1-x}Mn_xO$ coumpound. Within the GGA approach, one can demonstrate the appearance of a minority spin band gap. However, for d-character electrons, the calculated gap is signicantly reduced, states appearing around the Fermi level.

The substitution of a host semiconductor BaO by the transition metal atom Mn influence in the nature of the material, so, we notice that the gap of the minority spins decrease with increasing the concentration Mn, this substitution procedure opens a way to control the gap depending on our technological needs. According to our results, the material $Ba_{1-x}Mn_xO$ Keep the half-metallic behavior and is a good potential candidates in the technological application especially in the spintronic field.

REFERENCES

1. Z. Micković, EPFL Thesis no. 4728, "Study of diluted magnetic semiconductors: the case of transition metal doped ZnO" (2010). https://doi.org/10.5075/epfl-thesis-4728
2. S. Datta and B. Das, Appl. Phys. Lett. **56**, 665 (1990).
3. V. Ivády, I. A. Abrikosov, E. Janzén, and A. Gali, Phys. Rev. B **87**, 205201 (2013).
4. S. Methfessel and D. C. Mattis, *in Magnetism, Magnetic Semiconductors, vol. XVIII/1 of Encyclopedia of Physics*, 389562 (1968).
5. M. L. Reed, N. A. El-Masry, H. H. Stadelmaier, M. K. Ritum, and M. J. Reed, Appl. Phys. Lett. **79**, 3473 (2001).

6. E. Sarigiannidou, F. Wilhelm, E. Monroy, R. M. Galera, E. Bellet-Amalric, A. Rogalev, J. Goulon, J. Cibert, and H. Mariette, Phys. Rev. B **74**, 041306R (2006).
7. T. Graf, M. Gjukic, M. S. Brandt, and M. Stutzmann, "The $Mn^{3+=2+}$ acceptor level in group III nitrides," Appl. Phys. Lett. **81**, 5159 (2002).
8. H. Lakhdari, J. Supercond. Nov. Magn. **31**, No. 10 (2018).
9. H. Bahloul, J. Supercond. Nov. Magn. **31**, No. 12 (2018).
10. D. Misra and S. K. Yadav, Sci. Rep. **9**, 12593 (2019).
11. W. H. Strewlow and E. L. Cook, J. Phys. Chem. Ref. Data **2**, 163 (1973).
12. X. Yang, Y. Wang, Y. Chen, and H. Yan, Acta Phys. Pol., A **126**, 64 (2016).
13. J. A. McLeod, R. G. Wilks, N. A. Skorikow, L. D. Finkelstein, M. Abu-Samak, E. Z. Kurmaev, and A. Moewes, Phys. Rev. B **81**, 245123 (2010).
14. J. Junquera, M. Zimmer, P. Ordejón, and P. Ghosez, Phys. Rev. B **67**, 155327 (2003).
15. J. Kuneš, A. Lukoyanov, V. Anisimov, R. T. Scalettar, and W. E. Pickett, Nat. Mater. **7**, 198–202 (2008).
16. J. E. Pask, D. J. Singh, I. I. Mazin, C. S. Hellberg, and J. Kortus, Phys. Rev. B **64**, 024403
17. V. Solovyev, Phys. Rev. B **58**, 15496 (1998).
18. M. D. Towler, N. L. Allan, N. M. Harrison, V. R. Saunders, W. C. Mackrodt, and E. Apra, Phys. Rev. B **50**, 5041 (1994).
19. S. Massidda, A. Continenza, M. Posternak, and A. Baldereschi, Phys. Rev. Lett. **74**, 2323 (1995).
20. Fujimori, N. Kimizuka, T. Akahane, T. Chiba, S. Kimura, F. Minami, K. Siratori, M. Taniguchi, S. Ogawa, and S. Suga, Phys. Rev. B **42**, 7580 (1990).
21. T. Dietl, H. Ohno, F. Matsukura, J. Cibert, and D. Ferrand, Science **287**, 1019 (2000).
22. W. Kohn and L. J. Sham, Phys. Rev. **140**, 1133–1138 (1965).
23. Z. Wu and R. E. Cohen, Phys. Rev. B **73**, 1–6 (2006).
24. P. Blaha, K. Schwarz, G. K. H. Madsen, D. Kvasnicka, and J. Luitz, *WIEN2k, An Augmented Plane Wave C Local Orbitals Program for Calculating Crystal Properties*, Ed. by K. Schwarz (Technical Universitaet Wien, Wien, 2001).
25. P. Blaha, K. Schwarz, P. Sorantin, and S. B. Tricky, Comput. Phys. Commun. **59,** 399 (1990).
26. P. Blaha, K. Schwarz, G. K. H. Madsen, D. Kvasnicka, and J. Luitz. *WIEN2k, An Augmented Plane Wave + Local Orbitals Program for Calculating Crystal Properties* (Karlheinz Schwarz, Techn. Universitaet Wien, Wien, 2001).
27. K. Schwarz, P. Blaha, and G. K. H. Madsen, Comput. Phys. Commun. **147,** 71 (2002).
28. F. D. Muranghan, Proc. Natl. Acad. Sci. U.S.A. **30**, 244 (1944).
29. H. Lakhdari, B. Doumi, A. Mokaddem et al., J. Supercond. Nov. Magn. **32**, 1781 (2019).
30. K. L. Yao, G. Y. Gao, Z. L. Liu, and L. Zhu, Solid State Commun. **133**, 301 (2005).
31. Y. Gao, K. L. Yao, E. Şaşıoğlu, L. M. Sandratskii, Z. L. Liu, and J. L. Jiang, Phys. Rev. B **75**, 174442 (2007).
32. J. K. Furdyna, J. Appl. Phys. **64**, R29 (1988).
33. S. Sanvito, P. Ordejon, and N. A. Hill, Phys. Rev. B **63**, 165206 (2001).
34. H. Raebiger, A. Ayuela, and R. M. Nieminen, J. Phys.: Condens. Matter **16**, L457 (2004).